



## Article

# Study of Dynamic Viscoelasticity of a Mineral Oil-Based Magnetic Fluid

Zhanxian Li <sup>1,2</sup>, Yifei Guo <sup>1,2</sup> , Hujun Wang <sup>3,\*</sup>, Chengyao Deng <sup>4,5</sup> , Jiahao Dong <sup>4,5</sup>, Zhongru Song <sup>2</sup> and Zhenkun Li <sup>4,5,\*</sup>

- <sup>1</sup> Department of Mechanical Engineering, North China University of Science and Technology, Tangshan 063210, China; lizhanxian@ncst.edu.cn (Z.L.); gyf2710@126.com (Y.G.)
  - <sup>2</sup> Hebei Industrial Robot Industry Technology Research Institute, Tangshan 063000, China; szrtc@hotmail.com
  - <sup>3</sup> School of Applied, China University of Labor Relation, Beijing 100048, China
  - <sup>4</sup> School of Mechanical, Electronic and Control Engineering, Beijing Jiaotong University, Beijing 100044, China; 18221065@bjtu.edu.cn (C.D.); 20116012@bjtu.edu.cn (J.D.)
  - <sup>5</sup> Beijing Key Laboratory of Flow and Heat Transfer of Phase Changing in Micro and Small Scale, School of Mechanical, Electronic and Control Engineering, Beijing Jiaotong University, Beijing 100044, China
- \* Correspondence: wanghujun@sina.com (H.W.); zhkli@bjtu.edu.cn (Z.L.)

**Abstract:** Magnetic fluid is a field-responsive intelligent fluid, which has the flow characteristics of liquid and the elastic properties of solid. Because of its unique properties, it has a strong application prospect in the fields of magnetic soft robot, intelligent sensor, and so on. Dynamic viscoelasticity is a significant index to investigate the performance of magnetic fluid in the application process. In this paper, the dynamic viscoelasticity of a homemade mineral oil-based magnetic fluid was investigated under oscillatory shear experimental conditions using an MCR302 rheometer, and the effects of different temperatures and magnetic fields on the dynamic viscoelasticity were examined. Amplitude sweeps tests showed that the value of the storage modulus remained constant within the linear viscoelastic region (LVE) and the stable structure was not destroyed. As the magnetic field strength increased or the temperature increased, the range of the linear viscoelastic zone decreased. At large amplitude, the loss modulus will first appear as a peak and then decrease. The frequency sweep experiment showed that the storage modulus and loss modulus increased with the increase in angular frequency, and the greater the magnetic field intensity, the longer the internal structure relaxation time. When the magnetic field was constant, the higher the temperature, the smaller the storage modulus and loss modulus of the magnetic fluid. At high temperature, the loss coefficient of mesmeric fluid was large, and the magnetic fluid was more viscous. The lower the temperature is, the smaller the loss coefficient of the magnetic fluid is, and the magnetic fluid is more pliant. The study of dynamic viscoelasticity of magnetic fluids lays the foundation for establishing the complete structure intrinsic relationship of magnetic fluids and provides guidance for the application of magnetic fluids in magnetic 3D printing, droplet robot, and smart wear.

**Keywords:** magnetic fluid; viscosity; rheological properties



**Citation:** Li, Z.; Guo, Y.; Wang, H.; Deng, C.; Dong, J.; Song, Z.; Li, Z. Study of Dynamic Viscoelasticity of a Mineral Oil-Based Magnetic Fluid. *Magnetochemistry* **2023**, *9*, 143. <https://doi.org/10.3390/magnetochemistry9060143>

Academic Editor: Roberto Zivieri

Received: 24 April 2023

Revised: 24 May 2023

Accepted: 26 May 2023

Published: 29 May 2023



**Copyright:** © 2023 by the authors. Licensee MDPI, Basel, Switzerland. This article is an open access article distributed under the terms and conditions of the Creative Commons Attribution (CC BY) license (<https://creativecommons.org/licenses/by/4.0/>).

## 1. Introduction

Magnetic fluid, otherwise known as ferrofluid, is a stable colloidal suspension formed by fine ferromagnetic single-domain antiparticle in a non-conductive carrier fluid. When an external magnetic field is applicable, magnetic fluids exhibit a continuous, rapid reversible change from Newtonian fluid to Bingham-like, solidum-like solid state [1]. Back in 1963, Steve Papell of NASA invented a process to create magnetic fluids for liquid rocket fuel that can be brought into the inlet of a pump in a weightless environment by applying a magnetic field [2]. Under the action of a magnetic field, strong dipole interactions between particles lead to the formation of chain-like clusters in the direction of the magnetic field. This unique property provides the flexibility to control the fluid motion and improves the

functioning of the device. With continuous research on magnetic fluids, it was applied in various fields, such as targeted drug delivery, magnetosphere therapy of cancer cells, dampers, smart wear, magnetic field controlled 4D printing, and sealing [3–5].

Magnetic fluids are divided into ether-based, ester-based, kerosene-based, and mineral oil-based ferrite magnetic fluids according to their base carrier fluid, in which surface-modified ferrite magnetic particles show good dispersion in mineral oil [6] and have high magnetization strength, and mineral oil has high flash point and oxidation stability, which can make mineral oil-based magnetic fluids less prone to decomposition or oxidation at high temperatures or long-term use. Aromatic hydrocarbon-based mineral oil is a typical Newtonian fluid, in which the complete encapsulated magnetic particles are stably suspended. The non-Newtonian properties of the mesmeric formed fluid are mainly related to the anisotropic structure formed by the magnetic particles under the magnetic field, which is very suitable as a standard sample to study the rheological properties of magnetic fluids. Due to their good properties, mineral oil-based magnetic fluids are widely used in oil-filled transformers, medical imaging, lubrication, and other fields [7–10].

Magnetic fluid has certain viscoelasticity under the action of magnetic field. Viscoelasticity is divided into static viscoelasticity and dynamic viscoelasticity. Static viscoelasticity includes creep and stress relaxation. Dynamic viscoelasticity refers to the mechanical response of structured fluid under alternating strain or stress [11]. Relatively speaking, dynamic viscoelasticity is more suitable for studying the influence of fluid microstructure on mechanical properties. In dynamic viscoelasticity, the change of storage modulus  $G'$  and loss modulus  $G''$  is often used to represent the change of viscoelasticity of magnetic fluid. The storage modulus represents the elastic component of the viscoelastic modulus of the magnetic fluid, and the loss modulus represents the viscous component of the viscoelastic modulus of the magnetic fluid. Temperature, magnetic field strength, and shear rate are all factors affecting the viscoelasticity of magnetic fluid. Domestic and foreign scholars often use amplitude scanning experiments and frequency scanning experiments to study the dynamic viscoelasticity of magnetic fluids.

Yang et al. [12] developed a novel type of magnetic fluid through the dispersion of amorphous magnetic Fe-Ni-B nanoparticles into water colloid. The magnetorheological and viscoelastic properties of the magnetic fluid were subsequently explored. The findings demonstrate the occurrence of shear thinning behavior, and the viscoelastic aspects can be rationalized as the creation and rupture of chain or columnar structures. Sirimontree et al. [13] investigated the vibraphonist behavior of hollow multilateral cylindrical nutshells based on the theory of nonlocal elasticity, where the core layer is made of isotropic functional gradient material (FGM) and the other layers are made of magnetoelectric elastic material. The displacement field of the structure is exposed using the third-order shear deformation assumption (TSDA). The derivation of the vibraphonist equations in the form of coupling relations is achieved by implementing the Hamiltonian principle. Felicia et al. [14] attributed the viscoelasticity of magnetic fluids at different frequencies to the merging and splitting of the internal chain columnar structure of magnetic fluids, and used a microscopic rheological module to observe the columnar structure changes under rotational and oscillatory shear conditions of magnetic fluids, corroborating the hypothesis on the microscopic mechanism of viscoelasticity of magnetic fluids. Mishra et al. [15] confirmed the behavior of the solid–liquid crossover transition of magnetic fluids by dynamic oscillations of amplitude and frequent sweeps. Additionally, the amplitude required for the transition to increases with the increase in the particle size of the magnetic particles. Thus showing that the linear viscoelastic region increases with the increase in the particle size of the magnetic particles. Cunha et al. [16] investigated the effect of particle dipole interactions on the viscoelastic response of magnetic fluids and experimentally found that at the low frequency limit, dipole interactions increase the component of dynamic rotational viscosity, in addition to the crossover frequency of elastic jumps in magnetic fluids decreases with the increase of the dipole interaction parameter  $\lambda$ . Additionally, it was found that there are for two mechanisms for the formation of the elasticity of the constituent magnetic

fluids: the magnetic torque acting on each particle and the formation of particle aggregates, respectively. Yamaguchi et al. [17] investigated the effect of external magnetic field as well as magnetic particle concentration on dynamic viscoelasticity using a rheometer and experimentally showed that the applied magnetic field as well as particle concentration had a significant effect on dynamic viscoelasticity, with an increase in magnetic field significantly increasing the viscosity and elasticity of the magnetic fluid, while an increase in magnetic particle concentration greatly reduced the viscosity and elasticity of the magnetic fluid.

Scholars from various countries also explored the factors affecting the viscosity of magnetic fluids through a large number of experiments. Vinod et al. [18] mentioned in the review that the particle size and distribution of dispersed particles have a significant effect on the field-tunable thermal conductivity and rheology of ferromagnetic fluids. In the presence of a magnetic field, the thermal conductivity of the highly predisposed ferromagnetic fluid containing large aggregates is moderately enhanced, and the viscosity is greatly enhanced. Doganay et al. [19] mentioned in the review that in the presence of a magnetic field, some measurement results lead to a continuous increase in thermal conductivity and viscosity, but the remaining measurement results show that they first increase to a specific magnetic field value, and then they begin to decrease. Malekzadeh et al. [20] studied the viscosity of magnetic fluids containing  $\text{Fe}_3\text{O}_4$  magnetic particles. The results showed that the viscosity change depends on the volume fraction of nanoparticles, the temperature of magnetism and the intensity of the applied magnetic field. Higher nanoparticle volume fraction and lower nanofluid temperature exhibit higher viscosity. After applying an external magnetic field, the viscosity of the magnetic nanofluid increases. GU et al. [21] prepared water-based magnetic fluid by coating  $\text{Fe}_3\text{O}_4$  with SDBS. It was found that the viscosity of magnetic fluid increased with the increase in surfactant mass fraction, but also decreased with the increase in temperature. Moreover, the viscosity increases with the increase in magnetic field strength. Increasing temperature and surfactant mass fraction reduces the influence of magnetic field on the viscosity of magnetic fluid. Ryapolov et al. [22] found that when considering the state of magnetic fluid under a wide range of magnetic field and temperature parameters, the magnetoviscous effect includes the superposition of the input from the liquid colloid itself and its magnetic properties, which also depend not only on the applied magnetic field and temperature. The experimental methods and results mentioned in the above literature provided much help to carry out the experiments in this paper.

The measurement method is also the key to the success of the measurement. Wang et al. [23] used a torsional oscillating cup viscometer to study the viscosity of the self-made silicone oil-based magnetic fluid. The results showed that the viscosity of the magnetic fluid decreases with increasing temperature and increases with increasing magnetic field strength. Shel'deshova et al. [24] studied the magnetoviscous effect of magnetic fluid by analyzing the shear oscillation of magnetic fluid suspended in magnetic field. The results showed that the greatest influence on its rheological properties is the microstructure of the sample and the presence of large particles. Yang et al. [25] studied the magnetic viscosity of dilute iron fluid and concentrated iron fluid with a torsional oscillating cup viscometer. It was found that the relative magnetic viscosity hysteresis coefficient was positive in high magnetic field and negative in magnetic field under horizontal annular magnetic field. However, the above measurement methods have certain limitations in measuring the flow curve of magnetic fluid. In this paper, the rheological properties of magnetic fluid were measured by MCR302 rheometer.

The study of dynamic viscoelasticity of magnetic fluids can understand the changes of their microstructure under different experimental environments, provide a more thorough understanding of their molecular structure, and make due modifications to the molecular structure of magnetic fluids according to their application environments to maximize utilization. Dynamic viscoelasticity investigation experiments are an effective way to study the effect of microstructure of magnetic fluids on mechanical properties. In view of the limited experimental studies on the viscoelasticity of magnetic fluids in the existing

literature, the poor reproducibility, especially in frequency sweep studies, and the unclear mechanism of the effect of temperature on dynamic viscoelasticity, it is necessary to conduct an in-depth study on such properties of magnetic fluids.

In this paper,  $\text{Fe}_3\text{O}_4$  nanoparticles were prepared by co-precipitation method and coated and dispersed into L-AN46 mineral oil to prepare magnetic fluid. The structure, morphology, and magnetization properties of magnetic particles were studied. The static flow curves of L-AN46 based magnetic fluid were measured, and the relationship between viscosity and yield stress of L-AN46 based magnetic fluid and magnetic field and temperature was analyzed. The dynamic viscoelasticity of L-AN46 based magnetic fluids at different temperatures and magnetic fields was investigated by oscillatory shear theory and experimental methods, and amplitude sweep tests were used to demonstrate that the range and stability of the linear viscoelastic region of magnetic fluids are related to factors such as temperature and magnetic field. The strain rate frequency superposition principle was used to measure the complete frequency sweeps curves at different temperatures as well as at different magnetic fields, and the relaxation mechanism of the internal structure of magnetic fluids for different time scales was investigated according to the curve changes.

## 2. Experimental Method

### 2.1. Materials

In this paper, magnetic antiparticles of  $\text{Fe}_3\text{O}_4$  were produced by co-precipitation method,  $\text{FeCl}_3 \cdot 6\text{H}_2\text{O}$  and  $\text{FeCl}_2 \cdot 4\text{H}_2\text{O}$  were dissolved in water by heating a water bath at  $60^\circ\text{C}$  with stirring.

The beaker with the mixture was placed on a permanent magnet with a surface magnetic field strength of  $800\text{ kA/m}$  to precipitate the magnetic particles further, and the filtered precipitated magnetic powder was rinsed three times with ionized water. Filtered magnetic particles were dried in a high temperature drying oven.

To further analyze the  $\text{Fe}_3\text{O}_4$  particle size distribution, morphology of the prepared  $\text{Fe}_3\text{O}_4$  antiparticles was observed using electron microscopy (TEM). TEM images of the  $\text{Fe}_3\text{O}_4$  particles are shown in Figure 1a and the histograms of the particle size distribution are shown in Figure 1b. The observation results showed that the particle size of the prepared  $\text{Fe}_3\text{O}_4$  particles had a normal distribution and the average diameter was calculated to be  $10.36\text{ nm}$ .

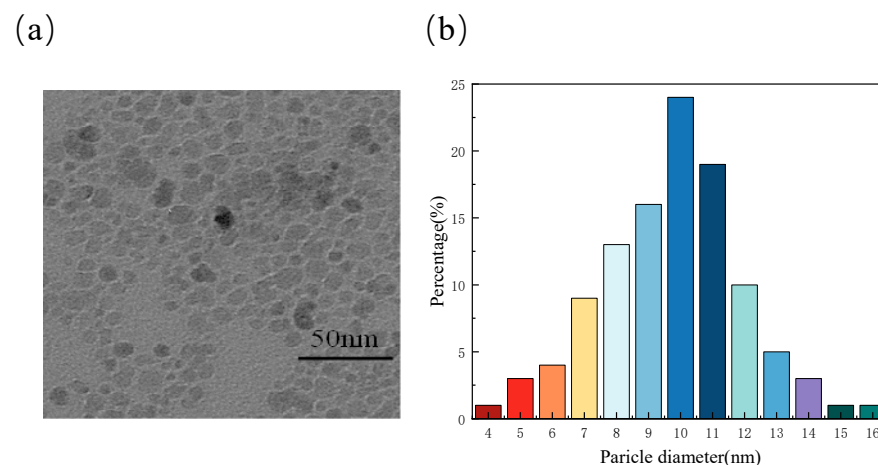


**Figure 1.** Particle size distribution diagram (a) TEM images of  $\text{Fe}_3\text{O}_4$  particles; (b) histogram of particle size distribution.

Magnetization curve of the  $\text{Fe}_3\text{O}_4$  magnetic particles prepared in this paper were measured using a Lakeshore 7404 vibrating sample magnetometer (VSM) shown in Figure 2. It can be seen that there was no obvious coercivity and remanence in the magnetization curve, which indicate that prepared  $\text{Fe}_3\text{O}_4$  particles are mainly small single-domain particles with

negligible content of large multi-domain particles. The saturation magnetization strength of the magnetic particles was determined to be 429 kA/m based on the curve stability value.

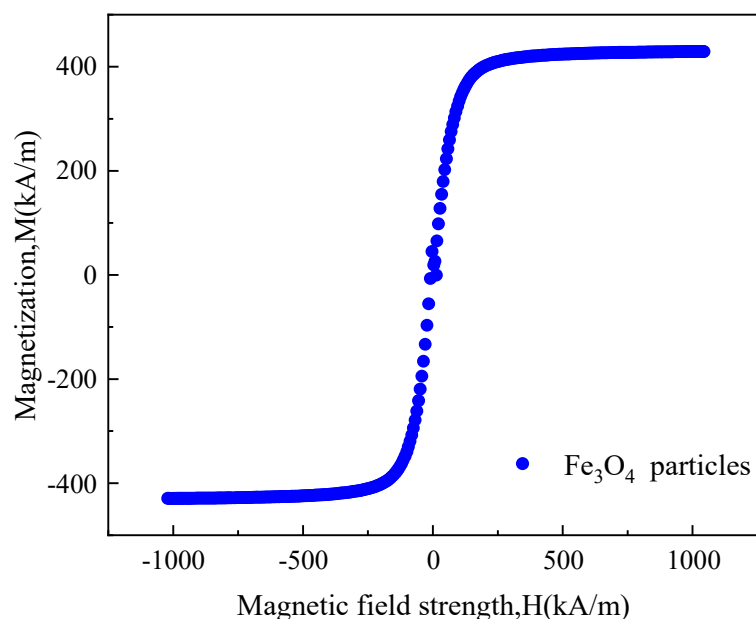


**Figure 2.** Magnetization curve of preparing  $\text{Fe}_3\text{O}_4$  magnetic particles.

In this experiment, China Petrochemical's L-AN46 total loss system oil was chosen as the basic carrier fluid of ferromagnetic fluid. GB443-1989 standard specifies 10 kinds of L-AN series total loss oils according to their different dynamic viscosity, and the basic parameters of L-AN46 total loss system oil are shown in Table 1.

**Table 1.** Basic physical parameters of L-AN46 base carrier fluid.

Mineral Oil	Kinematics Viscosity mPa·s (40 °C)	Flash Point °C	Pour Point °C	Density g/cm <sup>3</sup> (25 °C)
L-AN46	46	220	−28	0.858

The detailed preparation process of the oil-based magnetic fluid for the total loss system can be found in reference [26]. It is worth noting that during the preparation process, the volume ratio of the added magnetic particles to the base-loaded liquid and the stirring and ultrasonic dispersion time were strictly controlled. The physical parameters such as density, zero magnetic field viscosity, saturation magnetization intensity, and particle volume fraction of the magnetic fluid used in the experiments of this paper were summarized as showed in Table 2.

**Table 2.** Physical parameters of L-AN46-based carrier magnetic fluids.

Density g/cm <sup>3</sup>	Zero Magnetic Field Viscosity mPa·s (40 °C)	Saturation Magnetization kA/m	Particle Volume Fraction %
1.252	574.2	25.32	7.73

## 2.2. Experimental Setup

The MCR302 rotational rheometer manufactured by Anton Parr was selected for experimental study. The rheometer was equipped with MRD170 magnetic field module, which can generate a uniform magnetic field perpendicular to the disc surface, and the

module can generate a maximum magnetic field strength of 800 kA/m. A 20 mm diameter flat plate measurement rotor was selected and the rotor materials used in the measurement were all titanium alloy materials with a measurement gap of 0.2 mm during the rheological measurement. A simple diagram of the flat plate test system is shown in Figure 3.

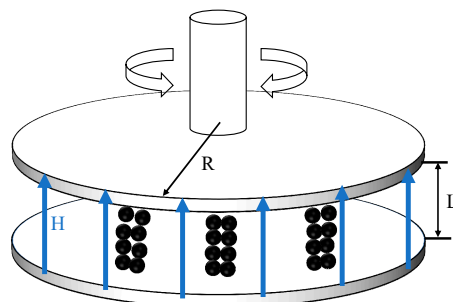


**Figure 3.** Simplified diagram of the flat plate measurement system.

This experiment investigated the effects of different magnetic field strength of the dynamic viscoelasticity of magnetic fluids at the same temperature, and the effects of different temperatures on the dynamic viscoelasticity of magnetic fluids at the same magnetic field strength. Amplitude sweeps tests and frequency sweep tests were utilized to investigate the effects of different conditions on the dynamic viscoelasticity of L-AN46based magnetic fluids.

In the oscillation experiments, the rheometer needs to be used to operate at a controlled shear rate for simplicity of mathematical calculations and the strain was applied using the sinusoidal function method. Applied small amplitude strain can be described as.

$$\gamma = \gamma_0 \cdot \sin(\omega \cdot t) \quad (1)$$

where  $\gamma_0$  is maximum strain (amplitude), %;  $\omega$ —angular frequency, rad/s;  $t$ —time, s.

The stresses within a complex fluid can be described as.

$$\tau = \tau_0 \sin(\omega t + \delta) \quad (2)$$

where  $\tau$ —maximum stress, Pa;  $\delta$ —phase difference.

The angular frequency is related to the oscillation frequency.

$$\omega = 2\pi \cdot f \quad (3)$$

where  $f$ —Frequency, Hz.

The total resistance of the material to the applied strain becomes the composite modulus  $G^*$ .

$$|G^*| = \tau_0 / \gamma_0 \quad (4)$$

The composite modulus  $G^*$  is defined as.

$$|G^*| = G' + iG'' \quad (5)$$

where  $G'$ -storage modulus, Pa;  $G''$ -loss modulus, Pa.

$$G' = G^* \cos \delta = \tau_0 / \gamma_0 \cdot \cos \delta \quad (6)$$

$$G'' = G^* \sin \delta = \tau_0 / \gamma_0 \cdot \sin \delta \quad (7)$$



### 3. Results and Discussion

#### 3.1. The Flow Curve

The flow curve reflects the rheological characteristics of the magnetic fluid as whole. Figure 4 is the flow curve of the magnetic fluid measured at a temperature of 20 °C and different magnetic field strength (25 mT, 50 mT, 75 mT, 100 mT, 125 mT). Before the start of the experiment, the sample was pre-sheared at a shear rate of 500 s<sup>-1</sup> for 5 min to eliminate the historical influence. The shear rate from 0.001 s<sup>-1</sup> to 100 s<sup>-1</sup> was applicable to the sample during the experiment. From the curve of Figure 4a, it can be clearly observed that the viscosity of the magnetic fluid gradually decreased with the increase in the shear rate, and there was an obvious shear thinning phenomenon. This shear thinning behavior was related to the complex structural changes inside the magnetic fluid. At first, there were many long chain structures in the magnetic fluid. With the increase in shear rate, the long chain structure became short chain structure, which led to the decrease of viscosity of the magnetic fluid. The relationship between shear stress and shear rate is shown in Figure 4b. It can be clearly observed that the shear stress increased with the increase in magnetic field strength. This was because the number of chain structures inside the magnetic fluid increased with the increase in magnetic field strength, and the yield stress of the magnetic fluid increased.

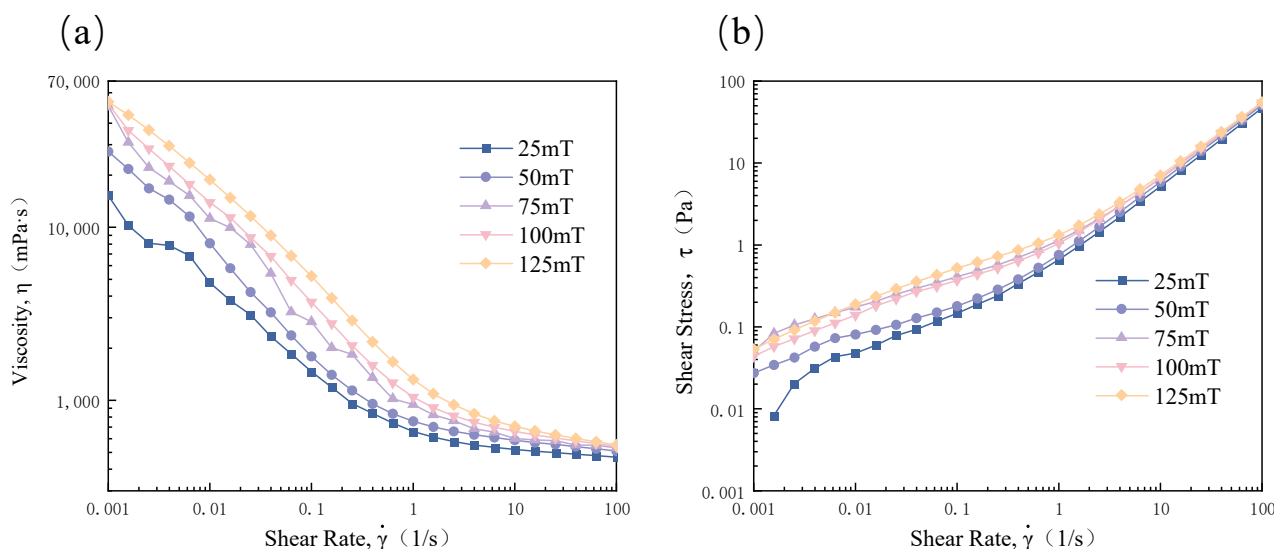


**Figure 4.** Flow curves of magnetic fluid under different magnetic fields: (a) the relationship between viscosity and shear rate; (b) the relationship between shear stress and shear rate.

Figure 5 is the flow curve of magnetic fluid under the condition of magnetic field intensity of 100 mT and different temperatures (10 °C, 20 °C, 30 °C, 40 °C). Before the start of the experiment, the sample was pre-sheared at a shear rate of 500 s<sup>-1</sup> for 5 min to eliminate the historical influence. The shear rate from 0.001 s<sup>-1</sup> to 100 s<sup>-1</sup> was applied to the sample during the experiment. It was observed from Figure 5a that the viscosity of magnetic fluid decreased with the increase in shear rate, and there was obvious shear thinning behavior. The higher the temperature is, the lower the viscosity is. This is because the Brownian thermal motion of the molecule was intense at high temperature. The force generated by the thermal motion of the molecule at high temperature was greater than the gravity generated by the magnetic field, resulting in a decrease in the number of stable chain structures inside the magnetic fluid. It was observed from Figure 5b that the shear stress increased with the increase in shear rate. The higher the temperature, the smaller the shear stress, the smaller the yield stress of the magnetic fluid.

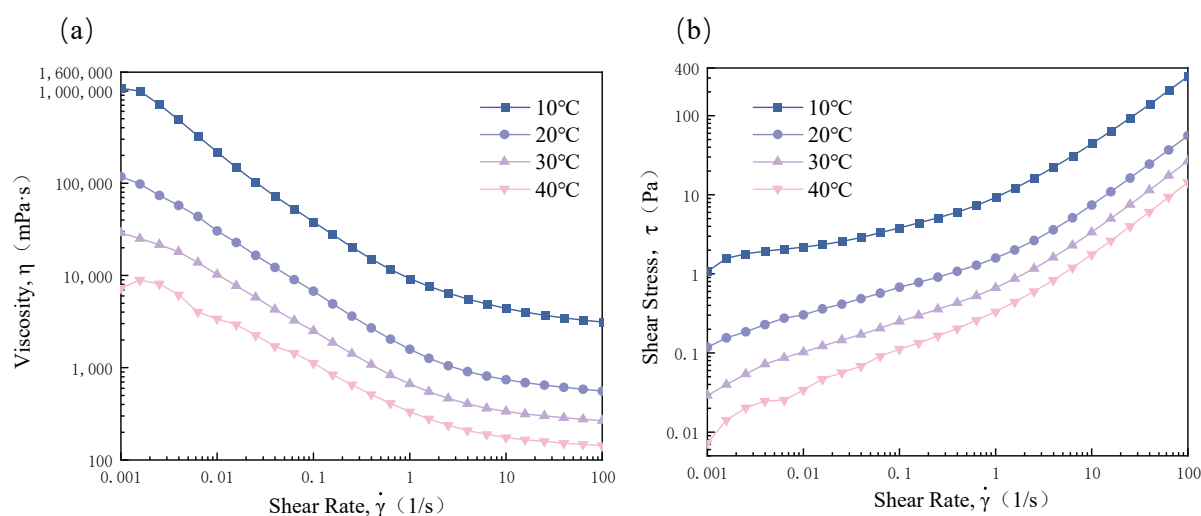


**Figure 5.** Flow curves of magnetic fluid under different temperature: (a) the relationship between viscosity and shear rate; (b) the relationship between shear stress and shear rate.

### 3.2. Amplitude Sweeps at Different Magnetic Field Strengths

The samples were first pre-sheared at a shear rate of  $500 \text{ s}^{-1}$  for 5 min to eliminate the effect of history before the experiments started, and the magnetic fluid was then left to stand in a magnetic field for 10 min to form a stable structure. In the amplitude sweep experiment, the oscillation frequency was controlled to be 5 rad/s constant frequency, and the amplitude changed from 0.01% to 100% under different magnetic field intensities (0 mT, 50 mT, 100 mT, 150 mT, 200 mT, 250 mT), and the experimental temperature is controlled at 25 °C.

The trends of the L-AN46-based magnetic fluid storage modulus and loss modulus measured by the amplitude sweep experiments are shown in Figure 6, and the changes in the modulus curves measured in the amplitude sweep experiments can determine the linear viscoelastic region of the test sample at small amplitudes and the nonlinear viscoelasticity at large amplitude oscillatory shear [27,28]. The linear viscoelastic zone represents the internal structure of complex fluids without damage. Beyond the linear viscoelastic zone, damage to the internal structure causes shear thinning of the complex fluid, and most of the applied energy is dissipated in the form of shear heat.

As shown in Figure 6a, the storage modulus  $G'$  loss modulus  $G''$  curves both increased with the increase in magnetic field strength, and at 1% strain the storage modulus increased from 0.19418 Pa at 0 mT to 56.31 Pa at 250 mT, which was due to the fact that with the increase in magnetic field strength, the chain structure connecting between the measurement plates laterally aggregated into a thick columnar structure, resulting in a significant increase in the storage modulus  $G'$  increases. As shown in Figure 6b, the loss modulus  $G''$  increased from 2.4699 Pa to 23.171 Pa when the magnetic field increased from 0 mT to 250 mT, which was due to the extensive distribution of some long chains of different lengths between the two measurement plates and a large number of much shorter chains with small gaps between the two plates, and the presence of these chains contributed to the increase in the loss modulus  $G''$ . From Figure 6a, it can be obtained that as the magnetic field strength increased, the linear viscoelastic zone gradually decreased, and as the magnetic field strength increased, more and more chains wound up to form a Chain-like structure with a larger diameter, which became more integral but less flexible, limiting the recoverable deflection angle of the columnar structure to a smaller range, and the columnar structure was easily destroyed at the connection of the measurement plate [24,29].



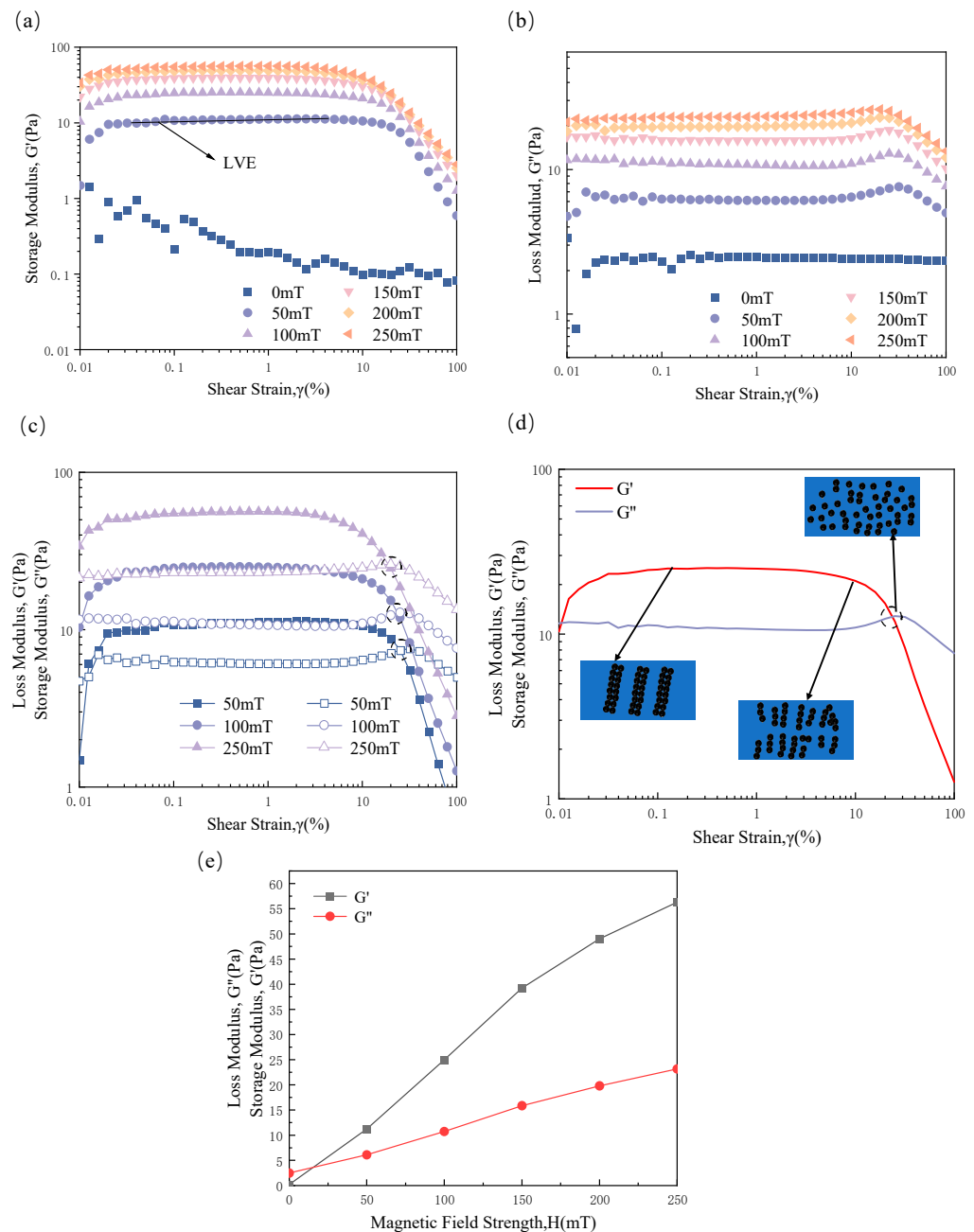


**Figure 6.** Plots obtained from amplitude sweep experiments at different magnetic field strengths: (a) relationship between amplitude and storage modulus at different magnetic field strengths; (b) relationship between amplitude and loss modulus at different magnetic field strengths; (c) modulus curves of L-AN46-based magnetic fluids at different magnetic field strengths (solid represents storage modulus, hollow represents loss modulus); (d) the change of internal microstructure of magnetic fluid in different stages of amplitude sweep (Black dots represents magnetic particles inside a magnetic fluid); (e) variation of the modulus within the linear viscoelastic zone with magnetic field strength.

Before the experiments, the magnetic fluid was pre-sheared and the magnetic particles were dispersed into a disordered distribution, which was free in the base carrier fluid and showed a Newtonian fluid characteristic with low viscosity. When resting under a magnetic field, the magnetic moment of magnetic particles inside the magnetic fluid was aligned along the magnetic field direction, and the particles form anisotropic chain and cluster structures under this interaction, and the chain and cluster structure [30] magnitudes

grew rapidly with the magnetic field strength, and lateral agglomeration occurred in the non-magnetic action, which made the magnetic fluid system further undergo phase transformation from a stable colloidal system to a thixotropic system, and finally formed a stable hexagonal equilibrium structure, when the internal storage modulus of the magnetic fluid was greater than the loss modulus, the magnetic fluid elasticity dominated, and the complex fluid was solid-like, showing the Bingham characteristic of high viscosity and low mobility (Bingham Fluid) [31].

As shown in Figure 6c, in the linear viscoelastic region, the columnar structure only deflected without being decomposed and destroyed, and the value of the storage modulus did not change. After the linear viscoelastic region was exceeded, part of the structure started to separate from the measured surface. At this stage, the microscopic columnar structure of the magnetic fluid was damaged. The deformation at this stage was inelastic and was not yet fully restored. As the amplitude continued to grow, the storage modulus  $G'$  curve intersected the loss modulus  $G''$  curve, resulting in an intersection of  $G_p$ . With the increase in magnetic field strength, the strength of the columnar structure inside the magnetic fluid became larger, and the yield stress also increased. When the amplitude was below  $G_p$ , the magnetic fluid exhibited solid-like or gel-like properties. When the amplitude exceeded  $G_p$ , the magnetic fluid was dominated by fluid viscous loss characteristics. There was a peak in the loss modulus  $G''$  curve near  $G_p$ , which corresponded to the energy dissipation generated when the stable structure inside the magnetic fluid was kept separated from the upper and lower surfaces of the measuring fixture. After that, the storage modulus  $G'$  and loss modulus  $G''$  continued to decrease, and the decrease rate of storage modulus  $G'$  was significantly higher than that of loss modulus  $G''$ . Finally, the viscous effect of magnetic fluid increased the recovery flow of magnetic fluid when the amplitude was large [32], which was linked to the decrease in the number of columnar structures with the increase in the amplitude. Figure 6d shows the changes in the internal microstructure of the magnetic fluid at different stages of the amplitude sweep.

Figure 6e shows the values of storage modulus and loss modulus measured in the linear viscoelastic zone with different magnetic field strengths. The growth rate of storage modulus  $G'$  was faster than that of loss modulus  $G''$  with increasing magnetic field strength, due to the increase in magnetization of the magnetic fluid with increasing magnetic field strength, the strength and number of magnetic induction chains and columnar structures, which led to the rapid increase in storage modulus  $G'$ . The slow growth of the loss modulus  $G''$  was due to the increase in the strength of the columnar structure with the increase in the magnetic field strength, the decrease in the relative flux between the magnetic particles and the carrier liquid, and the decrease in the friction loss. This, in turn, led to an increasing difference between the storage modulus  $G'$  and the loss modulus  $G''$  [33].

The corresponding relevant parameters in the amplitude sweep experiment are shown in Table 3:

**Table 3.** Corresponding relevant parameters in the amplitude sweep experiment.

Magnetic Field Strength (mT)	Range of LVE (%)	Storage Modulus of LVE (Pa)	$\tau$ of $G_p$ (Pa)
0	-	-	-
50	10	11.29	2.6369
100	6.31	24.972	4.4098
150	3.98	39.228	5.4511
200	2.51	49.016	6.5007
250	1.59	56.31	7.14556

### 3.3. Amplitude Sweeps at Different Temperatures

The samples were pre-sheared at a shear rate of  $500 \text{ s}^{-1}$  for 5 min to eliminate historical effects before the start of the experiment, followed by 10 min of resting in a magnetic field to form a stable structure. During the amplitude sweep experiment, the magnetic field

intensity was maintained at 100 mT, and the oscillation frequency was 5 rad/s constant frequency. The strain amplitude increased from 0.01% to 100% at different temperatures (0 °C, 5 °C, 10 °C, 15 °C, 20 °C, 25 °C, 30 °C, 35 °C, 40 °C). The change trend of storage modulus and loss modulus measured in the experiment is shown in Figure 7.

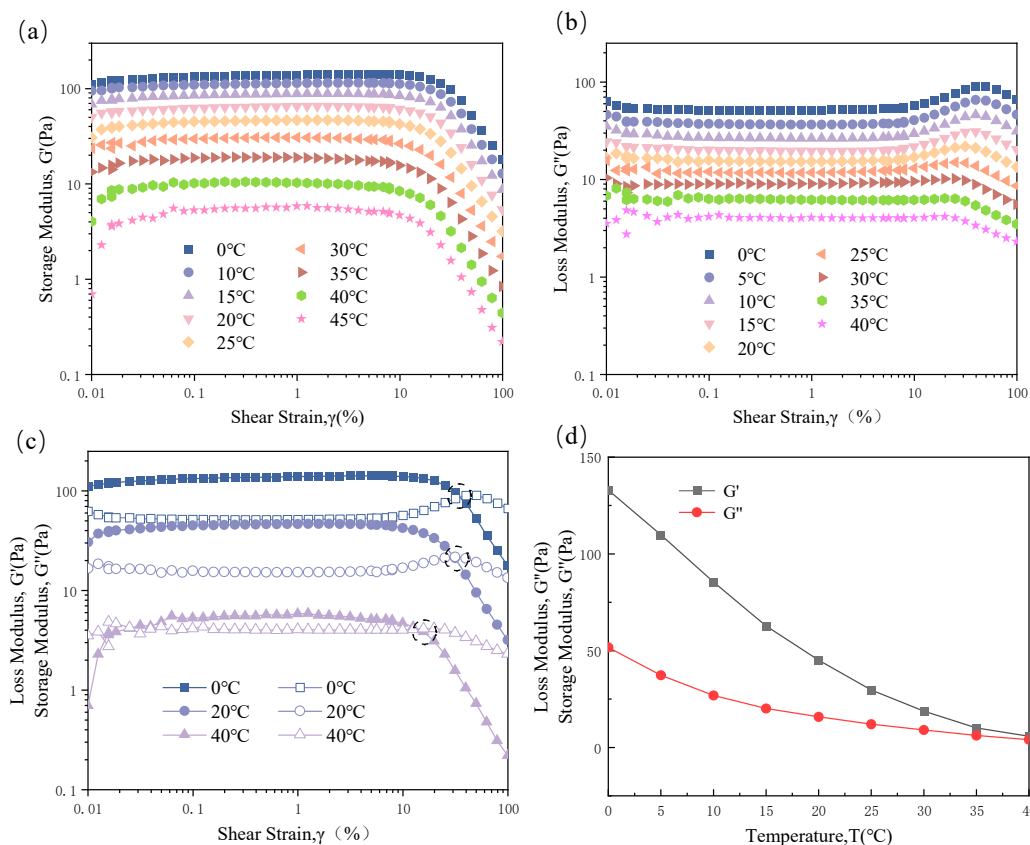


**Figure 7.** Plot of data in amplitude sweep experiments at different temperatures: (a) the relationship between storage modulus and amplitude at different temperatures; (b) the relationship between loss modulus and amplitude at different temperatures; (c) variation of modulus at different temperatures (solid represents storage modulus, hollow represents loss modulus); (d) variation of the modulus within the linear viscoelastic zone with magnetic field strength.

From Figure 7a,b, the storage modulus  $G'$  and loss modulus  $G''$  of L-AN46-based magnetic fluids decrease with increasing temperature due to the increase in free energy of the chain structure inside the magnetic fluid with increasing temperature, the easier separation of the columnar structure inside the magnetic fluid from the fixture surface, and the decrease in the number and size of the columnar structure inside the magnetic fluid with increasing temperature [34].

At low amplitude, the modulus curve of the magnetic fluid remained relatively stable in the linear viscoelastic region. Because of a small amplitude, there were a large number of columnar structures inside the magnetic fluid, and the columnar structure connecting the measuring plate can produce a larger deflection angle without damage before it was separated from the measuring plate. As the amplitude increased, the columnar structure inside the magnetic fluid was destroyed, resulting in a significant decrease in the storage modulus  $G'$ . When the amplitude was large, the magnetic fluid exhibited liquid characteristics.

It was observed from Figure 7b that the loss modulus  $G''$  curve will have a peak at larger amplitude, and the lower the temperature, the more obvious the peak. This peak represents the damage degree of the columnar structure in the magnetic fluid, and the more obvious structural damage is, the more obvious the peak is [35]. Because the lower the temperature, the more the columnar structure inside the magnetic fluid, the more stable the structure, the more noticeable the structure is destroyed, and the peak value of the

loss modulus  $G''$  curve is more obvious. With the increase in temperature, the number of columnar structures inside the magnetic fluid decreased, and the stability of the columnar structure decreased. Therefore, when the temperature was high, the columnar structure inside the magnetic fluid was not obviously damaged, resulting in the peak value of the loss modulus  $G''$  curve is not obvious.

Comparing the modulus curves at different temperatures in Figure 7c, it was observed that the linear viscoelastic region decreased with the increase in temperature, and it was observed in Figure 7d that in the linear viscoelastic region, as the temperature increased, the difference between the storage modulus  $G'$  and the loss modulus  $G''$  at the same temperature became smaller and smaller. The storage modulus  $G'$  decreased from 133 Pa to 5.8481 Pa, while the loss modulus  $G''$  decreased from 51.694 Pa to 4.0703 Pa. The decrease in storage modulus  $G'$  was about twice that of loss modulus  $G''$ . This was due to the increased temperature. The thermal Brownian motion of magnetic particles was intensified, and the viscous force of the basic carrier liquid was reduced. It was, therefore, difficult to form a chain structure due to the rapid movement of magnetic particles in the base carrier liquid. When the temperature increased, the number of chain structures inside the magnetic fluid reduced, resulting in a rapid decrease in the value of the storage modulus  $G'$ . Although the number of chain structures and columnar structures decreased with the increase in temperature, the storage modulus  $G'$  and the loss modulus  $G''$  reduced. However, with the decomposition of the chain and columnar structures inside the magnetic fluid, the loss modulus  $G''$  increased, resulting in a gentle decrease in the loss modulus  $G''$ .

### 3.4. Frequency Sweeps at Different Magnetic Field Strengths

The samples were pre-sheared for 5 min at  $500\text{ s}^{-1}$  to eliminate the effect of history before the start of the experiment, and they were then left to form a stable structure under a magnetic field for 10 min. The frequency sweep experiments were performed on L-AN46-based magnetic fluid under the controlled strain amplitude of 1% and the experimental temperature of  $25\text{ }^{\circ}\text{C}$ , and the oscillation frequency varied from  $0.1\text{ rad/s}$  to  $100\text{ rad/s}$  at different magnetic field strengths (50 mT, 75 mT, 100 mT, 150 mT, 200 mT). The change trend of storage modulus and loss modulus is shown in Figure 8.

As observed in Figure 8a,b, the values of the storage modulus  $G'$  and the loss modulus  $G''$  increased with the increase in the magnetic field strength, and the values of the storage modulus  $G'$  and the loss modulus  $G''$  increased with the increase in the oscillation frequency.

From Figure 8c, it was observed that the values of storage modulus  $G'$  and loss modulus  $G''$  became larger as the magnetic field strength increased for 50 mT, 75 mT, and 100 mT. The loss modulus  $G''$  was larger than the storage modulus  $G'$  at the beginning of the experiment, when the internal structure of the magnetic fluid can relax sufficiently to demonstrate the characteristic of mainly viscous loss. As the frequency increased, part of the structure was too late to relax, causing the  $G'$  curve representing the elastic component to grow significantly. At the lower oscillation frequency, the intersection of the storage modulus  $G'$  curve and the loss modulus  $G''$  curve occurs, and this intersection point represents the liquid–solid transition frequency of the magnetic fluid, and the reciprocal of this frequency was the characteristic relaxation time inside the complex fluid. It was also observed that the greater the magnetic field strength, the lower the frequency required for the intersection of the two curves, i.e., the longer the relaxation time of the internal structure of the magnetic fluid, and the magnetic fluid behaved in a colloidal state at this time, and this intersection point marked the beginning of the formation of a large columnar structure inside the magnetic fluid. In the frequency band between the first intersection and the second intersection, the storage modulus  $G'$  curve and the loss modulus  $G''$  curve grew smoothly, and as the frequency of oscillation increased, the storage modulus  $G'$  curve and the loss modulus  $G''$  curve intersected for the second time. The greater the magnetic field strength, the greater the frequency required for the second intersection to occur, indicating that the yield stress of the magnetic fluid became greater as the magnetic field

strength increased. At this time, the internal structure of complex fluid underwent a glassy turn, and the magnetic fluid mainly existed in the form of glassy state at high oscillation frequency, i.e., the magnetic fluid had both superior elasticity and viscosity. After this intersection point, the internal structure of the magnetic fluid tended to be more destructive than generative, so that the columnar structure was further decomposed, magnetic fluid underwent a flow phenomenon, and the viscous effect steadily increased. The value of loss modulus  $G''$  after the intersection was considerably higher than the value of storage modulus  $G'$ , which was related to the strong dissipation between complex structures under high frequency oscillation conditions.

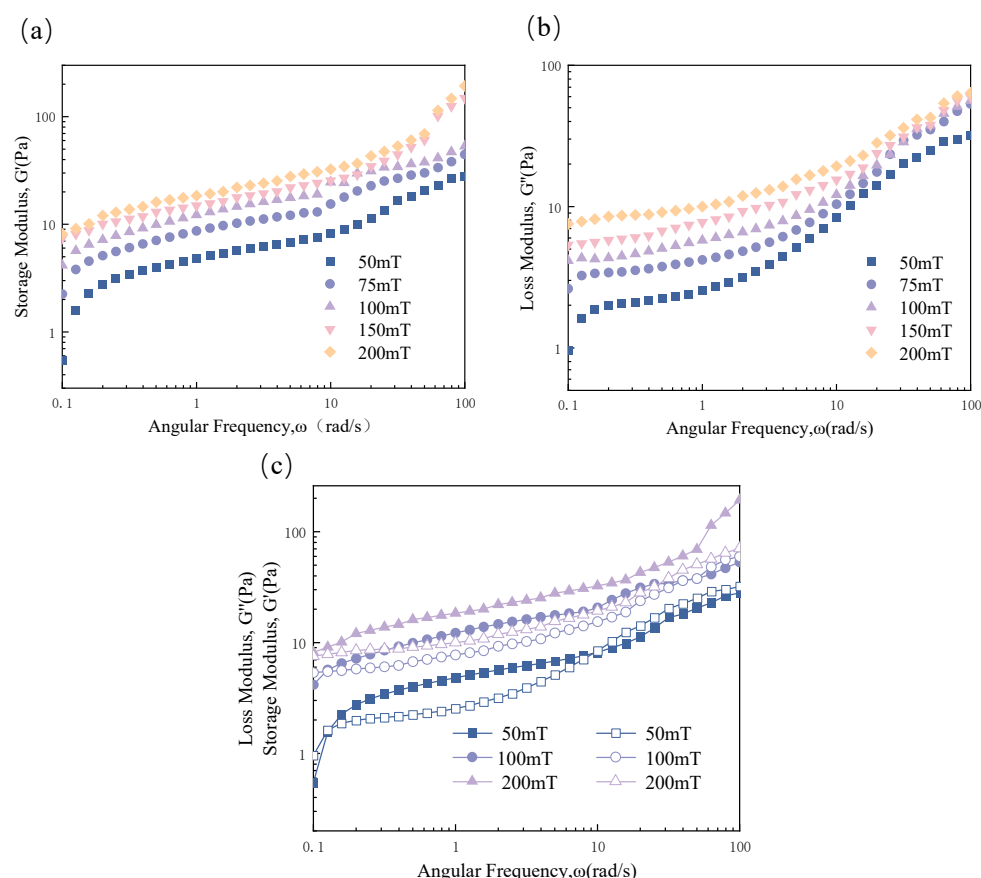


**Figure 8.** Plot of data in frequency sweep tests at different magnetic field strengths: (a) relationship between angular frequency and storage modulus at different magnetic field strengths; (b) relationship between angular frequency and loss modulus at different magnetic field strengths; (c) modulus change under different magnetic field strength (solid represents storage modulus, hollow represents loss modulus).

At magnetic field strengths of 150 mT and 200 mT, the storage modulus  $G'$  was always higher than the loss modulus  $G''$  during the experiment, which was due to the fact that at high magnetic field strengths, the magnetic fluid generated a stable columnar structure internally at the beginning of the experiment, and the tendency of columnar structure generation in oscillatory shear was much greater than that of destruction, and the shear force generated in the process of increasing frequency can never reach its yield force, when the complex fluid was dominated by elasticity.

### 3.5. Frequency Sweeps at Different Temperatures

The samples were pre-sheared for 5 min at  $500 \text{ s}^{-1}$  to eliminate the effect of history before the start of the experiment and were then rested under the magnetic field for 10 min to form a stable structure. The frequency sweep experiment of L-AN46-based magnetic fluid was carried out under the control of the strain amplitude value of 5% and the experimental

magnetic field strength of 100 mT. The oscillation frequency changed from 0.1 rad/s to 100 rad/s at different magnetic field strengths (0 °C, 5 °C, 10 °C, 15 °C, 20 °C, 25 °C, 30 °C, 35 °C). The change trend of storage modulus and loss modulus is shown in Figure 9.

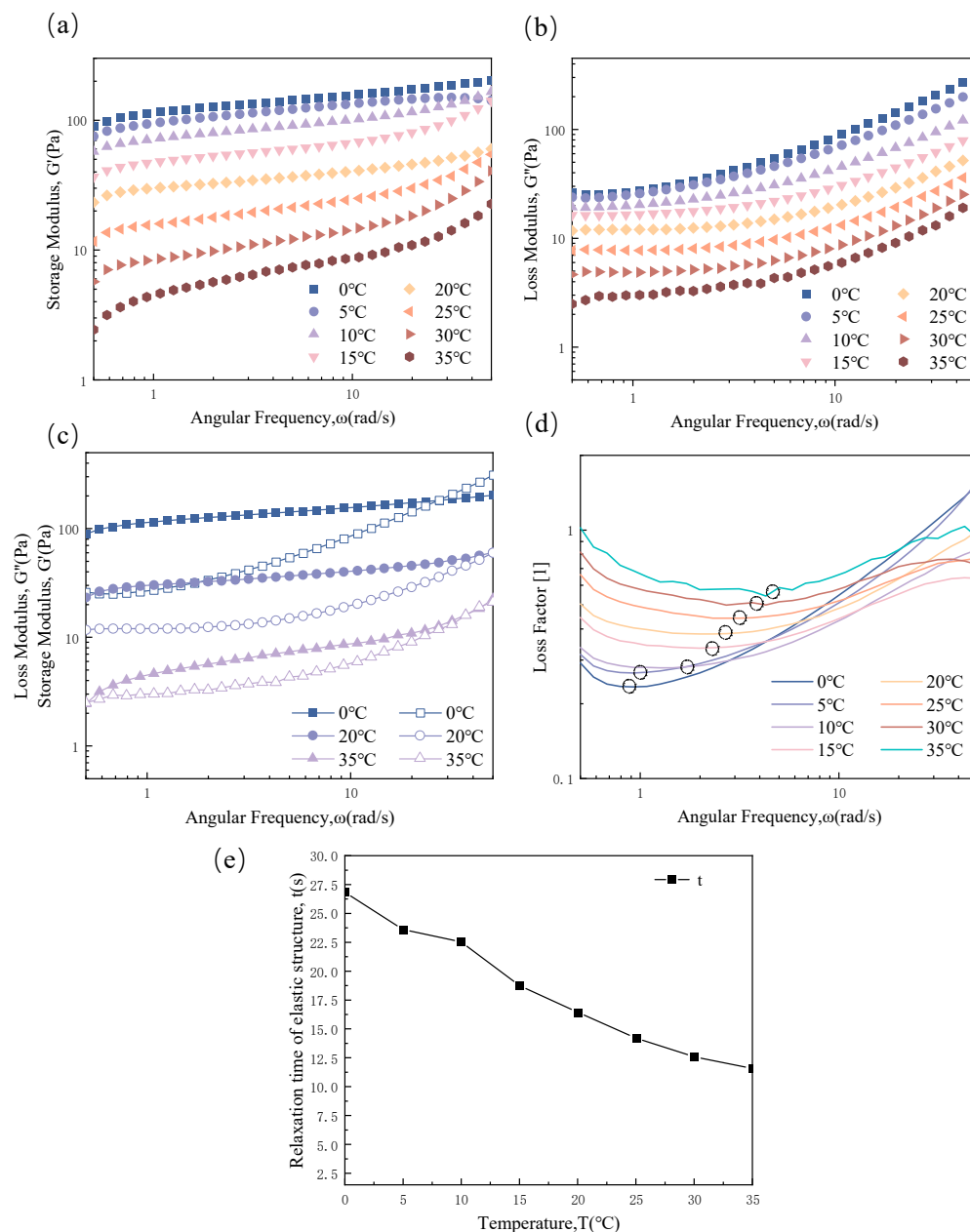


**Figure 9.** Plot of data in frequency sweep tests at different temperatures: (a) relationship between storage modulus and angular frequency at different temperatures; (b) relationship between loss modulus and angular frequency at different temperatures; (c) variation of modulus in frequency sweep tests at different temperatures (solid represents storage modulus, hollow represents loss modulus); (d) relationship between angular frequency and loss coefficient at different temperatures; (e) the relationship between relaxation time and temperature of the most elastic structure.

As shown in Figure 9a,b, it was observed that the values of storage modulus  $G'$  and loss modulus  $G''$  of the magnetic fluid increased with the increase in angular frequency, and the direction of chain structure inside the magnetic fluid under oscillatory shear was distributed along the shear direction, and the increase in oscillatory frequency led to more entanglement of chain structures in the base carrier liquid because the deformation of molecular chains could not keep up with the change of shear force. However, due to



the increase in temperature, the Brownian motion of magnetic particles in the magnetic fluid increased, and the viscosity of the base carrier liquid decreased, so the free magnetic particles were less likely to gather, resulting in the decrease in the number of chain structures inside the magnetic fluid at high temperature. At low temperature, the force generated by the magnetic field was much larger than the force of Brownian motion, so the number of columnar structures inside the magnetic fluid was high and the stability was higher, resulting in high values of storage modulus  $G'$  and loss modulus  $G''$  of the magnetic fluid and the spacing between the two curves is larger.

From Figure 9c, it was observed that the magnetic fluid was more elastic at low frequencies, which appeared in a decreasing trend of the loss coefficient curve in Figure 9d. At this time, the magnetic fluid was in a solid-like state, and as the angular frequency increases, the growth trend of the storage modulus  $G'$  was lower than the growth trend of the loss modulus  $G''$ , at which time the loss coefficient curve, as shown in Figure 9d, showed an upward trend. Subsequently, the two straight lines intersected, when the internal microstructure of the magnetic fluid underwent a vitrification transition [36], indicating that the magnetic fluid existed in the form of vitrification under high frequency oscillations, i.e., there was a high viscosity and elasticity at the same time, and the value of the loss modulus  $G''$  was always higher than the storage modulus  $G'$  with the increase in the oscillation frequency, as shown in Figure 9d, where the loss coefficient was greater than 1. This was explained by the fact that under the high frequency oscillation conditions, the internal complex fluid structure was strongly dissipated.

In Figure 9d, the frequency corresponding to the lowest point of each curve corresponded to the most elastic structural state inside the magnetic fluid, and the most expandable structure was the largest columnar structure in the whole experimental process. The reciprocal of the lowest frequency was the relaxation time of the large columnar structure, as illustrated in Figure 9e. The higher the temperature is, the shorter the relaxation time is. The higher the temperature is, the smaller the internal columnar structure of the magnetic fluid is. The connection of magnetic particles in the columnar structure was unstable, and the thermal molecular motion accelerated the relaxation of the columnar structure. The lower the temperature, the larger the columnar structure, the more intricate the magnetic particle connection inside the magnetic fluid, the more stable the columnar structure, and the longer the relaxation time.

#### 4. Conclusions

We studied the dynamic viscoelasticity of self-made magnetic fluid by steady shear and oscillatory shear. The results showed that the magnetic fluid had obvious shear thinning behavior during steady shear. The viscosity of the magnetic fluid increased with the increase in the magnetic field and decreased with the increase in temperature.

In the amplitude sweep, the linear viscoelastic region of the magnetic fluid decreased with the increase in the magnetic field, and the linear viscoelastic region decreased from 10% to 1.59%. The higher the magnetic field, the higher the storage modulus  $G'$  and loss modulus  $G''$  of the magnetic fluid. During the experiment, the storage modulus  $G'$  increased from 0.6802 Pa to 53.055 Pa with the increase in magnetic field strength, and the loss modulus  $G''$  increased from 2.331 Pa to 22.742 Pa. However, as the temperature increased, the Brownian motion of the particles increased, resulting in a decrease in the stability of the columnar structure inside the magnetic fluid. As the temperature increased, the linear viscoelastic region of the magnetic fluid shrank from 9.93% to 1.98%. The storage modulus  $G'$  decreased from 123.95 Pa to 3.854 Pa, and the loss modulus  $G''$  decreased from 52.408 Pa to 3.6931 Pa.

In the frequency sweep, the values of the storage modulus  $G'$  and the loss modulus  $G''$  increased with the increase in the angular frequency, regardless of the different magnetic field strength or different temperature. During the experiment, with the increase in magnetic field, the storage modulus  $G'$  increased from 0.5465 Pa to 8.1417 Pa at low frequency, and the loss modulus  $G''$  increased from 0.958 Pa to 7.5372 Pa. However, the storage modu-

lus  $G'$  and the loss modulus  $G''$  of the magnetic fluid will decrease at high temperature. As the temperature increased, the storage modulus  $G'$  decreased from 89.298 Pa to 2.4393 Pa, and the loss modulus  $G''$  decreased from 26.057 Pa to 2.4925 Pa. The frequency sweep results showed that the larger the magnetic field strength or the lower the temperature, the longer the relaxation time of the internal structure of the magnetic fluid, and the earlier the liquid–solid conversion will occur. However, the second intersection will appear later, indicating that the magnetic fluid undergoes different microstructure evolution paths in frequency sweep under different magnetic field strengths or different temperatures.

The research on the rheological properties of mineral oil-based magnetic fluids in this paper provides help for magnetic 3D printing, magnetic fluid robots, intelligent wear, and other technologies.

**Author Contributions:** Conceptualization, Z.L. (Zhanxian Li); methodology, Z.L. (Zhenkun Li); formal analysis, H.W.; investigation, Y.G. and C.D.; data curation, Y.G.; writing—original draft preparation, Y.G.; writing—review and editing, Z.L. (Zhenkun Li) and H.W.; supervision, Z.L. (Zhenkun Li), J.D. and Z.S.; project administration, Z.L. (Zhenkun Li); funding acquisition, Z.L. (Zhenkun Li) All authors have read and agreed to the published version of the manuscript.

**Funding:** This work was supported by the Fundamental Research Funds for the Central Universities (No. 2021RC278).

**Institutional Review Board Statement:** Not applicable.

**Informed Consent Statement:** Not applicable.

**Data Availability Statement:** Data are available from the authors upon reasonable request.

**Conflicts of Interest:** The authors declare no conflict of interest.

## References

1. Kaloni, P.N.; Mahajan, A. Stability and uniqueness of ferrofluids. *Int. J. Eng. Sci.* **2010**, *48*, 1350–1356. [\[CrossRef\]](#)
2. Behera, A.; Behera, A. Smart Fluid. In *Advanced Materials: An Introduction to Modern Materials Science*; Springer: Berlin/Heidelberg, Germany, 2022; pp. 193–223.
3. Pankhurst, Q.A.; Connolly, J.; Jones, S.K.; Dobson, J. Applications of magnetic nanoparticles in biomedicine. *J. Phys. D-Appl. Phys.* **2003**, *36*, R167–R181. [\[CrossRef\]](#)
4. Zhang, Y.; Jiang, S.; Hu, Y.; Wu, T.; Zhang, Y.; Li, H.; Li, A.; Zhang, Y.; Wu, H.; Ding, Y.; et al. Reconfigurable Magnetic Liquid Metal Robot for High-Performance Droplet Manipulation. *Nano Lett.* **2022**, *22*, 2923–2933. [\[CrossRef\]](#)
5. Pathak, S.; Jain, K.; Noorjahan, Kumar, V.; Pant, R.P. Magnetic Fluid Based High Precision Temperature Sensor. *IEEE Sens. J.* **2017**, *17*, 2670–2675. [\[CrossRef\]](#)
6. Viali, W.R.; Alcantara, G.B.; Sartoratto, P.P.C.; Soler, M.A.G.; Mosiniwicz-Szablewska, E.; Andrzejewski, B.; Morais, P.C. Investigation of the Molecular Surface Coating on the Stability of Insulating Magnetic Oils. *J. Phys. Chem. C* **2010**, *114*, 179–188. [\[CrossRef\]](#)
7. Yadav, N.; Jarial, R.K.; Rao, U.M. Characterization of Mineral oil Based  $\text{Fe}_3\text{O}_4$  Nanofluid for Application in Oil Filled Transformers. *Int. J. Electr. Eng. Inform.* **2018**, *10*, 338–349. [\[CrossRef\]](#)
8. Muangpratoom, P.; Pattanadech, N. Dielectric Breakdown Strength of Mineral Oil Based Nanofluids. In Proceedings of the 2016 International Conference on Condition Monitoring and Diagnosis (CMD), Xi'an, China, 25–28 September 2016; Xi'an Jiaotong University: Xi'an, China, 2016; pp. 266–269.
9. Huang, W.; Wang, X. Ferrofluids lubrication: A status report. *Lubr. Sci.* **2016**, *28*, 3–26. [\[CrossRef\]](#)
10. Chen, S.; Wang, J.; Lu, H.; Xu, L. Surfactant-Modified Silica Nanoparticles-Stabilized Magnetic Polydimethylsiloxane-in-Water Pickering Emulsions for Lubrication and Anticorrosion. *ACS Sustain. Chem. Eng.* **2022**, *10*, 10816–10826. [\[CrossRef\]](#)
11. Ferry, J.D. *Viscoelastic Properties of Polymers*; John Wiley & Sons: Hoboken, NJ, USA, 1980.
12. Yang, C.; Li, T.; Pei, X.; Li, J.; Yuan, Z.; Li, Y.; Bian, X. Magnetorheological and Viscoelastic Behaviors in an Fe-Based Amorphous Magnetic Fluid. *Materials* **2023**, *16*, 1967. [\[CrossRef\]](#)
13. Sirimontree, S.; Thongchom, C.; Saffari, P.R.; Refahati, N.; Saffari, P.R.; Jearsiripongkul, T.; Keawsawasvong, S. Effects of thermal environment and external mean flow on sound transmission loss of sandwich functionally graded magneto-electro-elastic cylindrical nanoshell. *Eur. J. Mech. A/Solids* **2023**, *97*, 104774. [\[CrossRef\]](#)
14. Felicia, L.J.; Philip, J. Probing of Field-Induced Structures and Tunable Rheological Properties of Surfactant Capped Magnetically Polarizable Nanofluids. *Langmuir* **2013**, *29*, 110–120. [\[CrossRef\]](#)

15. Mishra, A.; Pathak, S.; Kumar, P.; Singh, A.; Jain, K.; Chaturvedi, R.; Singh, D.; Basheed, G.; Pant, R. Measurement of static and dynamic magneto-viscoelasticity in facile varying pH synthesized  $\text{CoFe}_2\text{O}_4$ -based magnetic fluid. *IEEE Trans. Magn.* **2019**, *55*, 1–7. [\[CrossRef\]](#)
16. Cunha, F.R.; Rosa, A.P. Effect of particle dipolar interactions on the viscoelastic response of dilute ferrofluids undergoing oscillatory shear. *Phys. Fluids* **2021**, *33*, 092004. [\[CrossRef\]](#)
17. Yamaguchi, H.; Niu, X.-D.; Ye, X.-J.; Li, M.; Iwamoto, Y. Dynamic rheological properties of viscoelastic magnetic fluids in uniform magnetic fields. *J. Magn. Magn. Mater.* **2012**, *324*, 3238–3244. [\[CrossRef\]](#)
18. Vinod, S.; Philip, J. Thermal and rheological properties of magnetic nanofluids: Recent advances and future directions. *Adv. Colloid Interface Sci.* **2022**, *307*, 102729. [\[CrossRef\]](#) [\[PubMed\]](#)
19. Doganay, S.; Alsangur, R.; Turgut, A. Effect of external magnetic field on thermal conductivity and viscosity of magnetic nanofluids: A review. *Mater. Res. Express* **2019**, *6*, 112003. [\[CrossRef\]](#)
20. Malekzadeh, A.; Pouranfard, A.R.; Hatami, N.; Kazemnejad Banari, A.; Rahimi, M.R. Experimental investigations on the viscosity of magnetic nanofluids under the influence of temperature, volume fractions of nanoparticles and external magnetic field. *J. Appl. Fluid Mech.* **2016**, *9*, 693–697. [\[CrossRef\]](#)
21. Gu, H.; Tang, X.; Hong, R.; Feng, W.; Xie, H.; Chen, D.; Badami, D. Ubbelohde viscometer measurement of water-based  $\text{Fe}_3\text{O}_4$  magnetic fluid prepared by coprecipitation. *J. Magn. Magn. Mater.* **2013**, *348*, 88–92. [\[CrossRef\]](#)
22. Ryapolov, P.A.; Shel'deshova, E.V.; Postnikov, E.B. Temperature and field dependences of magnetic fluid's shear viscosity: Decoupling inputs from a carrier fluid and magnetic nanoparticles. *J. Mol. Liq.* **2023**, *382*, 121887. [\[CrossRef\]](#)
23. Wang, S.; Yang, C.; Bian, X. Magnetoviscous properties of  $\text{Fe}_3\text{O}_4$  silicon oil based ferrofluid. *J. Magn. Magn. Mater.* **2012**, *324*, 3361–3365. [\[CrossRef\]](#)
24. Shel'deshova, E.; Churaev, A.; Ryapolov, P. Dynamics of Magnetic Fluids and Bidisperse Magnetic Systems under Oscillatory Shear. *Fluids* **2023**, *8*, 47. [\[CrossRef\]](#)
25. Yang, C.; Bian, X.; Qin, J.; Zhao, X.; Zhang, K.; Bai, Y. An investigation of a viscosity-magnetic field hysteretic effect in nano-ferrofluid. *J. Mol. Liq.* **2014**, *196*, 357–362. [\[CrossRef\]](#)
26. Li, Z.; Li, D.; Chen, Y.; Cui, H. Study of the thixotropic behaviors of ferrofluids. *Soft Matter* **2018**, *14*, 3858–3869. [\[CrossRef\]](#) [\[PubMed\]](#)
27. Jahan, N.; Pathak, S.; Jain, K.; Pant, R.P. Enhancement in viscoelastic properties of flake-shaped iron based magnetorheological fluid using ferrofluid. *Colloids Surf. A-Physicochem. Eng. Asp.* **2017**, *529*, 88–94. [\[CrossRef\]](#)
28. Pang, H.; Pei, L.; Sun, C.; Gong, X. Normal stress in magnetorheological polymer gel under large amplitude oscillatory shear. *J. Rheol.* **2018**, *62*, 1409–1418. [\[CrossRef\]](#)
29. Xuan, Y.; Huang, Y.; Li, Q. Experimental investigation on thermal conductivity and specific heat capacity of magnetic microencapsulated phase change material suspension. *Chem. Phys. Lett.* **2009**, *479*, 264–269. [\[CrossRef\]](#)
30. Li, Z.; Li, D.; Hao, D.; Cheng, Y. Study on the creep and recovery behaviors of ferrofluids. *Smart Mater. Struct.* **2017**, *26*, 105022. [\[CrossRef\]](#)
31. Dong, J.; Li, D.; Li, Z. Different methods for determining the yield stress of ferrofluids. *J. Intell. Mater. Syst. Struct.* **2023**, *34*, 800–810. [\[CrossRef\]](#)
32. Denn, M.M.; Bonn, D. Issues in the flow of yield-stress liquids. *Rheol. Acta* **2011**, *50*, 307–315. [\[CrossRef\]](#)
33. Wang, G.; Geng, J.; Guo, T.; Qi, X.; Yu, R.; Zhang, Z.; Wang, Y.; Wang, Z.; Li, Z.; Li, P. Magneto-stimuli rheological response of hierarchical  $\text{Fe}_3\text{O}_4$  submicron spheres for high performance magnetorheological fluid. *Ceram. Int.* **2022**, *48*, 29031–29038. [\[CrossRef\]](#)
34. Fan, Y.; Xie, L.; Yang, W.; Sun, B. Magnetic field dependent viscoelasticity of a highly stable magnetorheological fluid under oscillatory shear. *J. Appl. Phys.* **2021**, *129*, 204701. [\[CrossRef\]](#)
35. Ibiyemi, A.A.; Yusuf, G.T.; Olusola, A. Influence of temperature and magnetic field on rheological behavior of ultra-sonicated and oleic acid coated cobalt ferrite ferrofluid. *Phys. Scr.* **2021**, *96*, 125842. [\[CrossRef\]](#)
36. Lacoste, D.; Lubensky, T.C. Phase transitions in a ferrofluid at magnetic-field-induced microphase separation. *Phys. Rev. E* **2001**, *64*, 041506. [\[CrossRef\]](#) [\[PubMed\]](#)

**Disclaimer/Publisher's Note:** The statements, opinions and data contained in all publications are solely those of the individual author(s) and contributor(s) and not of MDPI and/or the editor(s). MDPI and/or the editor(s) disclaim responsibility for any injury to people or property resulting from any ideas, methods, instructions or products referred to in the content.